EARTHQUAKE ENGINEERING AND STRUCTURAL DYNAMICS
Earthquake Engng Struct. Dyn. (in press)
Published online in Wiley InterScience (www.interscience.wiley.com). DOI: 10.1002/eqe.453

Forced vibration testing of buildings using the linear shaker seismic simulation (LSSS) testing method

Eunjong Yu[1], Daniel H. Whang[2,*,†], Joel P. Conte[3], Jonathan P. Stewart[1] and John W. Wallace[1]

[1]*Department of Civil and Environmental Engineering, University of California, Los Angeles, CA, U.S.A.*
[2]*Department of Civil and Environmental Engineering, University of Auckland, Auckland, New Zealand*
[3]*Department of Structural Engineering, University of California, San Diego, CA, U.S.A.*

SUMMARY

This paper describes the development and numerical verification of a test method to realistically simulate the seismic structural response of full-scale buildings. The result is a new field testing procedure referred to as the linear shaker seismic simulation (LSSS) testing method. This test method uses a linear shaker system in which a mass mounted on the structure is commanded a specified acceleration time history, which in turn induces inertial forces in the structure. The inertia force of the moving mass is transferred as dynamic force excitation to the structure. The key issues associated with the LSSS method are (1) determining for a given ground motion displacement, x_g, a linear shaker motion which induces a structural response that matches as closely as possible the response of the building if it had been excited at its base by x_g (i.e. the motion transformation problem) and (2) correcting the linear shaker motion from Step (1) to compensate for control–structure interaction effects associated with the fact that linear shaker systems cannot impart perfectly to the structure the specified forcing functions (i.e. the CSI problem). The motion transformation problem is solved using filters that modify x_g both in the frequency domain using building transfer functions and in the time domain using a least squares approximation. The CSI problem, which is most important near the modal frequencies of the structural system, is solved for the example of a linear shaker system that is part of the NEES@UCLA equipment site. Copyright © 2005 John Wiley & Sons, Ltd.

KEY WORDS: linear shaker; full-scale seismic simulation; servo-hydraulic actuator model; control–structure interaction; proportional-derivative control; delta pressure feedback

INTRODUCTION

Field performance data from full-scale structural systems have been a principal driving force behind advances in earthquake engineering practice since the early 20th century. For example,

*Correspondence to: Daniel H. Whang, University of Auckland, Private Bag 92019, Auckland, New Zealand.
†E-mail: dwhang@auckland.ac.nz

Contract/grant sponsor: National Science Foundation: George E. Brown, Jr. Network for Earthquake Engineering Simulation (NEES) Program; contract/grant number: CMS-0086596

Received 3 October 2003
Revised 8 July 2004
Accepted 3 November 2004

observations of structural collapse following the 1933 Long Beach earthquake led to some of the first formal recommendations on earthquake resistant design and retrofitting of existing structures [1]. More recently, observations of building performance following the 1971 San Fernando, 1989 Loma Prieta and 1994 Northridge earthquakes provided the impetus for major building code revisions in the 1976, 1985, 1991 and 1997 versions of the Uniform Building code (UBC, 1976, 1985, 1991, and 1997). The weight given to field performance data stems from a simple fact: it represents the 'ground truth' information against which all analysis procedures, code provisions, and other tests results must be calibrated.

Field performance data in structures can be generated either by seismic excitation or forced vibration testing. The focus here is on forced vibration testing of full-scale structures. Advantages of field testing relative to laboratory testing include the lack of need for scaling, correct boundary conditions, and lack of interactions between the specimen and the testing apparatus/facility. However, several factors have limited the impact of field testing to date, including:

(1) The inability of artificial (forced) vibration sources to test structures at large amplitudes, and in particular, in their non-linear range.
(2) The inability of traditional vibration sources to excite structures in a manner that emulates realistic broadband seismic excitation.
(3) Practical difficulties associated with deploying a sufficiently dense sensor array such that detailed component behavior can be investigated.

The NSF-funded George E. Brown, Jr. Network for Earthquake Engineering Simulation (NEES) project at UCLA has addressed each of these issues by developing large capacity harmonic eccentric shakers, a linear servo-hydraulic inertial shaker able to reproduce broadband seismic excitation, and a field data acquisition system with IP-based wireless telemetry that enables convenient deployment of large sensor arrays.

This paper focuses on the second issue identified above: the development of a linear broadband shaker system to provide structural excitations that realistically simulate linear elastic structural seismic response. The theoretical framework for the proposed test method is developed and illustrated with a numerical example. The result is a new field testing procedure referred to as the linear shaker seismic simulation (LSSS) testing method. LSSS represents a fifth type of test method to investigate the seismic response of structural systems; the other methods being quasi-static cyclic, pseudodynamic, shake table and effective force testing [2].

DESCRIPTION OF THE LSSS METHOD

During an earthquake, a building is subjected to inertial forces caused by a ground motion $x_g(t)$. As shown in Figure 1(a), the effect of base excitation on a building is equivalent to that of a set of effective earthquake lateral forces applied to the building on a stationary base. These effective earthquake forces depend on the building inertia properties and the earthquake ground acceleration. In contrast, forced vibration experiments are typically designed such that the mechanical shakers are anchored to the roof of the test structure. Consequently, vibrations induced during forced vibration experiments and earthquakes emanate from opposite locations—'top excitation' during forced vibration experiments and 'base excitation' during earthquakes. The lateral force distributions induced during the two cases are different since

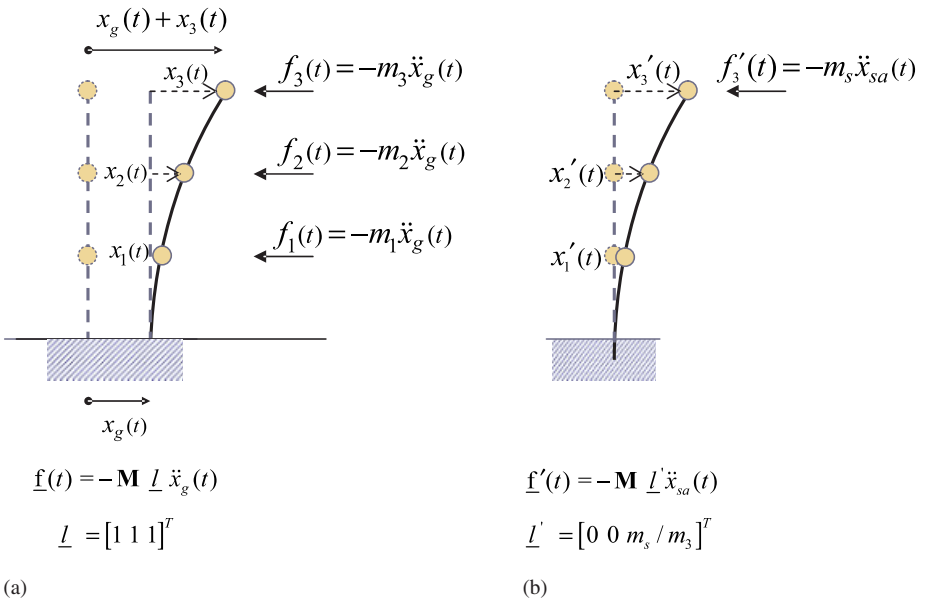

Figure 1. Comparison of effective force distributions for earthquake excitation and shaker excitation; (a) base excitation; and (b) top excitation.

the linear shakers can only apply an inertial force to the floor where they are attached. This difference can be described in terms of the influence vector, $\underline{l}$, which defines the degrees-of-freedom affected by the external excitation [3] as follows:

$$\underline{\mathrm{f}}(t) = -\mathbf{M}\underline{l}\ddot{x}_{\mathrm{a}}(t) \tag{1}$$

where $\underline{\mathrm{f}}(t)$ = effective lateral force vector, $\mathbf{M} = (n \times n)$ mass matrix of the building, $\underline{l} = (n \times 1)$ influence vector, $\ddot{x}_{\mathrm{a}}(t)$ = applied acceleration history due to either the ground motion ($\ddot{x}_{\mathrm{a}}(t) = \ddot{x}_{\mathrm{g}}(t)$) or shaker excitation ($\ddot{x}_{\mathrm{a}}(t) = \ddot{x}_{\mathrm{sa}}(t)$, where $\ddot{x}_{\mathrm{sa}}(t)$ = absolute shaker acceleration), and n = number of dynamic degrees-of-freedom in the building. The difference in the $\underline{l}$ vectors for the base and top excitation cases is illustrated in Figure 1 for a 3-story building model with one translational degree-of-freedom per floor.

In Figure 1 and Equation (1), $x_{\mathrm{sa}}(t)$ is the absolute displacement of the moving mass m_{s} of the linear shaker, and m_i is the mass of floor level i in the building. The displacement $x_{\mathrm{sa}}(t)$ is distinguished in Figure 2 from the displacement of the roof relative to the base $x_n(t)$ and the displacement of the shaker mass relative to the roof $x_{\mathrm{s}}(t)$.

Clearly, if the same acceleration history was applied for the base and top excitation cases (i.e. $\ddot{x}_{\mathrm{sa}}(t) = \ddot{x}_{\mathrm{g}}(t)$), different structural responses would be induced. Accordingly, the first major challenge associated with the development of the LSSS testing method is to determine for a given ground motion, $x_{\mathrm{g}}(t)$, a linear shaker input motion which induces a structural response that matches as closely as possible (in the linear elastic range) the response of the building if it had been excited at its base by $x_{\mathrm{g}}(t)$. Two alternative solutions to this motion transformation problem are presented. The first approach filters the ground motion $x_{\mathrm{g}}(t)$ in the frequency domain using building transfer functions, while the second approach

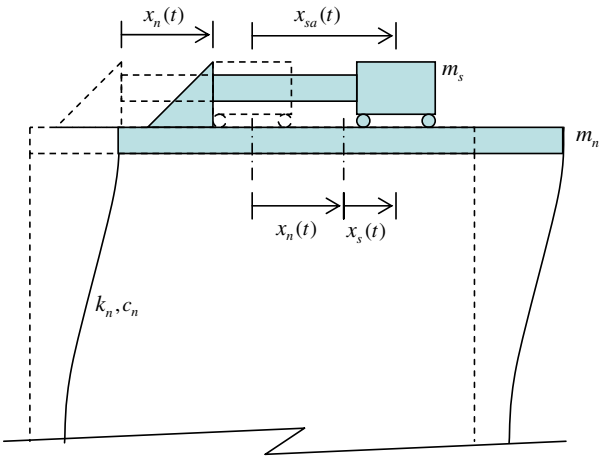

Figure 2. Definition of displacement quantities for linear shaker on a test structure.

modifies the forcing function in the time domain using a least squares approximation. Both of the motion transformation methods assume that the linear shaker can reproduce the specified forcing function exactly (i.e. perfect control system). As shown later, this assumption is not always realistic. For example, experimental studies by Dyke *et al.* [4] and Dimig *et al.* [2] have shown that servo-hydraulic actuators attached to lightly damped structures are limited in their ability to apply forces near the test structure's natural frequencies. Consequently, the second challenge in developing the LSSS test method is to account for imperfect hydraulic actuator control by pre-correcting the shaker input motion that would be obtained under the assumption of a perfect control system (i.e. the control–structure interaction problem). In the following sections, mathematical solutions to the motion transformation and control–structure interaction problems are described.

THE MOTION TRANSFORMATION PROBLEM

LSSS transfer function method

The equation of motion of an elastic n degrees-of-freedom building structure subjected to a lateral force vector $\underline{\mathrm{f}}(t)$ can be expressed as

$$\mathbf{M}\ddot{\underline{\mathrm{x}}}(t) + \mathbf{C}\dot{\underline{\mathrm{x}}}(t) + \mathbf{K}\underline{\mathrm{x}}(t) = \underline{\mathrm{f}}(t) \tag{2}$$

where $\underline{\mathrm{x}}(t) = (n \times 1)$ displacement vector relative to the base, and $\mathbf{M}$, $\mathbf{C}$ and $\mathbf{K} = (n \times n)$ mass, damping and stiffness matrices, respectively. Assuming zero initial conditions, the Laplace transformation of Equation (2) yields:

$$[\mathbf{M}s^2 + \mathbf{C}s + \mathbf{K}]\underline{\mathrm{X}}(s) = \underline{\mathrm{F}}(s) \tag{3}$$

where

$$\underline{\mathrm{X}}(s) = L\{\underline{\mathrm{x}}(t)\} = \int_0^\infty \mathrm{e}^{-st}\underline{\mathrm{x}}(t)\,\mathrm{d}t \tag{4a}$$

$$\underline{\mathrm{F}}(s) = L\{\underline{\mathrm{f}}(t)\} = \int_0^\infty \mathrm{e}^{-st}\underline{\mathrm{f}}(t)\,\mathrm{d}t \tag{4b}$$

in which s denotes the Laplace domain parameter, which is related at poles to both system modal frequencies and damping ratios [5]. The transfer function matrix $\mathbf{H}(s)$ transforms the input forcing function $\underline{\mathrm{F}}(s)$ into the output vector $\underline{\mathrm{X}}(s)$, i.e.

$$\underline{\mathrm{X}}(s) = \mathbf{H}(s)\underline{\mathrm{F}}(s) \tag{5}$$

and is defined as the following $(n \times n)$ matrix:

$$\mathbf{H}(s) = [\mathbf{M}s^2 + \mathbf{C}s + \mathbf{K}]^{-1} = \begin{bmatrix} H_{11} & H_{12} & \dots & H_{1n} \\ & H_{22} & \dots & H_{2n} \\ & & \ddots & \vdots \\ \text{sym.} & & & H_{nn} \end{bmatrix} \tag{6}$$

A unique transfer function exists for the output (displacement) at the i-th DOF due to the input (force) at the j-th DOF, which is represented by the $H_{ij}(s)$ component of $\mathbf{H}(s)$. Using Equation (5), the dynamic response of a linear elastic structure can be derived using the inverse Laplace transformation of $\underline{\mathrm{X}}(s)$,

$$\underline{\mathrm{x}}(t) = L^{-1}\{\underline{\mathrm{X}}(s)\} = L^{-1}\{\mathbf{H}(s)\underline{\mathrm{F}}(s)\} \tag{7}$$

Since the displacement response of the i-th floor [$x_i(t)$ or $X_i(s)$] is the superposition of the responses associated with inputs applied at each floor, the displacement $X_i(s)$ can be expressed by the sum (over the number of floors) of the product of transfer functions and floor inputs. Representing the input by the equivalent lateral force vector $\underline{\mathrm{F}}(s)$ (i.e. Laplace transform of the $\underline{\mathrm{f}}(t)$ vector in Figure 1), displacement responses $X_i(s)$ and $X_i'(s)$ for base and shaker excitation, respectively, are given by:

$$\text{Base excitation:} \quad X_i(s) = \sum_{j=1}^{n} H_{ij}(s)F_j(s) = -\sum_{j=1}^{n} H_{ij}(s)m_j\ddot{X}_{\mathrm{g}}(s) \tag{8}$$

$$\text{Shaker excitation:} \quad X_i'(s) = \sum_{j=1}^{n} H_{ij}(s)F_j'(s) = -\sum_{j=1}^{n} H_{ij}(s)m_j l_j'\ddot{X}_{\mathrm{sa},j}(s) \tag{9}$$

where $F_j(s)$ and m_j represent the effective earthquake force and the story mass at floor j, respectively, $\ddot{X}_{\mathrm{g}}(s)$ is the Laplace transformation of the ground motion and is equivalent to $s^2X_{\mathrm{g}}(s)$, and l_j' is the j-th component of influence vector $\underline{l}'$. For the special case of excitation applied only at the roof level (i.e. $j = n$ only), the summation in Equation (9) reduces to

$$\text{Top Excitation:} \quad X_i'(s) = -H_{in}(s)m_{\mathrm{s}}\ddot{X}_{\mathrm{sa}}(s) \tag{10}$$

where $H_{in}(s)$ is the transfer function between the shaker input on floor level n and the displacement response of the i-th floor.

Equating Equations (8) and (10), the linear shaker input motion $\ddot{X}_{\mathrm{sa}}(s)$ that will induce an i-th floor response, $X_i'(s)$, that will match $X_i(s)$ from the base excitation can be derived using a filter $T(s)$ defined as

$$\ddot{X}_{\mathrm{sa}}(s) = T(s)\ddot{X}_{\mathrm{g}}(s) \tag{11}$$

$$T(s) = \frac{\sum_{j=1}^{n} H_{ij}(s)m_j}{H_{in}(s)m_{\mathrm{s}}} \tag{12}$$

Finally, the shaker input motion $\ddot{x}_{\mathrm{sa}}(t)$ is obtained as

$$\ddot{x}_{\mathrm{sa}}(t) = L^{-1}\{\ddot{X}_{\mathrm{sa}}(s)\} = L^{-1}\{T(s)\ddot{X}_{\mathrm{g}}(s)\} \tag{13}$$

In this approach, the shaker input motion $\ddot{x}_{\mathrm{sa}}(t)$ is obtained through a filter defined as the ratio of two transfer functions such that the responses of the i-th floor due to the base excitation and top excitation will coincide. Note that $T(s)$ depends on which aspect (DOF) of the response is being matched. This method can be extended to replicate alternative response quantities such as total base shear, story overturning moment, or inter-story drift. However, a shortcoming of this approach is its inability to match simultaneously the response of multiple DOFs (or multiple response quantities).

LSSS least squares method

From the governing equation of the MDOF dynamic system response subjected to base excitation (Equation (2) with $\underline{\mathrm{f}}(t)$ evaluated as shown in Figure 1(b)), the discrete form of the solution can be found using the Newmark Explicit method [6, 7] as follows:

$$\underline{\mathrm{x}}(k+1) = \underline{\mathrm{x}}(k) + \Delta t\dot{\underline{\mathrm{x}}}(k) + \tfrac{1}{2}\Delta t^2\ddot{\underline{\mathrm{x}}}(k) \tag{14a}$$

$$\dot{\underline{\mathrm{x}}}(k+1) = \dot{\underline{\mathrm{x}}}(k) + \tfrac{1}{2}\Delta t[\ddot{\underline{\mathrm{x}}}(k) + \ddot{\underline{\mathrm{x}}}(k+1)] \tag{14b}$$

Substituting Equations (14) into Equation (2), and introducing the structural response vector, $\underline{z}$, results in the following discrete state equation [7]:

$$\underline{\mathrm{z}}(k+1) = \mathbf{A}\underline{\mathrm{z}}(k) + \underline{\mathrm{L}}\ddot{x}_{\mathrm{g}}(k+1) \tag{15}$$

where

$$\underline{\mathrm{z}}(k) = \begin{bmatrix} \underline{\mathrm{x}}(k) \\ \Delta t\dot{\underline{\mathrm{x}}}(k) \\ \Delta t^2\ddot{\underline{\mathrm{x}}}(k) \end{bmatrix} \tag{16a}$$

$$\mathbf{A} = \begin{bmatrix} \mathbf{I} & \mathbf{I} & \tfrac{1}{2}\mathbf{I} \\ -\tfrac{1}{2}\Delta t^2\hat{\mathbf{M}}^{-1}\mathbf{K} & \mathbf{I} - \tfrac{1}{2}[\Delta t\hat{\mathbf{M}}^{-1}\mathbf{C} + \Delta t^2\hat{\mathbf{M}}^{-1}\mathbf{K}] & \tfrac{1}{2}\left[\mathbf{I} - \tfrac{1}{2}\Delta t\hat{\mathbf{M}}^{-1}\mathbf{C}\right] - \tfrac{1}{4}\Delta t^2\hat{\mathbf{M}}^{-1}\mathbf{K} \\ -\Delta t^2\hat{\mathbf{M}}^{-1}\mathbf{K} & -\Delta t\hat{\mathbf{M}}^{-1}\mathbf{C} - \Delta t^2\hat{\mathbf{M}}^{-1}\mathbf{K} & -\tfrac{1}{2}\Delta t\hat{\mathbf{M}}^{-1}\mathbf{C} - \tfrac{1}{2}\Delta t^2\hat{\mathbf{M}}^{-1}\mathbf{K} \end{bmatrix} \tag{16b}$$

$$\underline{\mathrm{L}} = \begin{bmatrix} \underline{0} \\ \frac{1}{2}\Delta t^2 \hat{\mathbf{M}}^{-1}\mathbf{M}\underline{l} \\ \Delta t^2 \hat{\mathbf{M}}^{-1}\mathbf{M}\underline{l} \end{bmatrix} \tag{16c}$$

$$\hat{\mathbf{M}} = \mathbf{M} + \tfrac{1}{2}\mathbf{C}\Delta t \tag{16d}$$

In the above equations, Δt is the constant time step, $\mathbf{I}$ is the $(n \times n)$ identity matrix, $\ddot{x}_g(k+1)$ is the ground acceleration at discrete time $t_{k+1} = (k+1)\Delta t$, and $\underline{0}$ is an $(n \times 1)$ vector of zeros. Column vector $\underline{z}(k)$ is referred to as the structural response vector at discrete time $t = k\Delta t$ and has length $3n$, as does vector $\underline{\mathrm{L}}$. The response of the structure subjected to top excitation can be expressed similarly as

$$\underline{z}'(k+1) = \mathbf{A}\underline{z}'(k) + \underline{\mathrm{L}}'\ddot{x}_{sa}(k+1) \tag{17}$$

where $\underline{z}'(k+1)$ and $\ddot{x}_{sa}(k+1)$ represent the structural response vector and shaker acceleration at time t_{k+1} in the case of top excitation, and $\underline{\mathrm{L}}'$ is determined using the influence vector $\underline{l}'$ instead of $\underline{l}$ in Equation (16c). System matrix $\mathbf{A}$ has dimensions of $(3n \times 3n)$ and is identical for both the base and top excitation cases. Since the response of the system at time t_N is the superposition of the responses to the individual inputs at time t_k, $k = 0, 1, \ldots, N$, the difference in the structural response between base and top excitation cases at time step $t = t_N$ can be expressed as

$$\underline{\varepsilon}(N) = \underline{z}(N) - \underline{z}'(N) = \underline{z}(N) - [(\mathbf{A})^N \underline{\mathrm{L}}'\ddot{x}_{sa}(0) + (\mathbf{A})^{N-1}\underline{\mathrm{L}}'\ddot{x}_{sa}(1) + \cdots + \underline{\mathrm{L}}'\ddot{x}_{sa}(N)] \tag{18}$$

The error vector $\tilde{\underline{\varepsilon}}$ is then introduced as

$$\tilde{\underline{\varepsilon}} = \begin{Bmatrix} \underline{\varepsilon}(1) \\ \underline{\varepsilon}(2) \\ \vdots \\ \underline{\varepsilon}(N) \end{Bmatrix} = \begin{Bmatrix} \underline{z}(1) \\ \underline{z}(2) \\ \vdots \\ \underline{z}(N) \end{Bmatrix} - \begin{bmatrix} \mathbf{L}' & \underline{0} & \cdots & \underline{0} \\ \mathbf{A}\mathbf{L}' & \mathbf{L}' & \cdots & \underline{0} \\ \vdots & \vdots & \ddots & \vdots \\ (\mathbf{A})^{N-1}\mathbf{L}' & (\mathbf{A})^{N-2}\mathbf{L}' & \cdots & \mathbf{L}' \end{bmatrix} \begin{Bmatrix} \ddot{x}_{sa}(1) \\ \ddot{x}_{sa}(2) \\ \vdots \\ \ddot{x}_{sa}(N) \end{Bmatrix} \tag{19a}$$

or

$$\tilde{\underline{\varepsilon}} = \underline{z} - \mathbf{G}\ddot{\underline{x}}_{sa} \tag{19b}$$

where the dimensions of $\tilde{\underline{\varepsilon}}$, $\underline{z}$, $\mathbf{G}$, and $\ddot{\underline{x}}_{sa}$ are $(3nN \times 1)$, $(3nN \times 1)$, $(3nN \times N)$, and $(N \times 1)$, respectively. Matrix $\mathbf{G}$ is defined by Equation (19). Therefore, the linear shaker input motion $\ddot{\underline{x}}_{sa}$ which minimizes the error between $\underline{z}$ and $\underline{z}'$ can be derived by minimizing the L_2 (or Euclidean) norm of the errors from time t_1 to t_N, which can be expressed as

$$\min\|\tilde{\underline{\varepsilon}}\|_2 = \min\|\underline{z} - \mathbf{G}\ddot{\underline{x}}_{sa}\|_2 \tag{20}$$

where $\|\cdot\|_2$ denotes the L_2 norm of a vector.

A closed form solution to Equation (20) can be found using the least squares method, which is equivalent to minimizing the sum of the squared errors from t_1 to t_N,

$$\|\tilde{\underline{\varepsilon}}\|_2^2 = (\underline{z} - \mathbf{G}\ddot{\underline{x}}_{sa})^{\mathrm{T}}(\underline{z} - \mathbf{G}\ddot{\underline{x}}_{sa}) \tag{21}$$

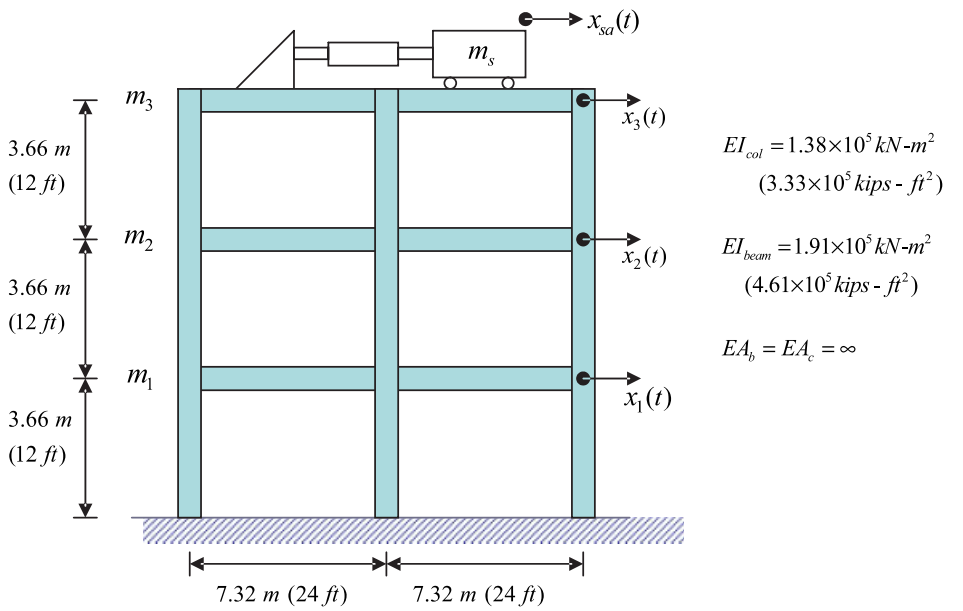

Figure 3. Three-story, two-bay example building.

Taking the derivatives of Equation (21) with respect to the shaker input acceleration, $\underline{\ddot{x}}_{sa}$, and setting the result equal to zero (i.e. the minimization problem), it is found that

$$(-\mathbf{G}^T)(\underline{z} - \mathbf{G}\underline{\ddot{x}}_{sa}) = \underline{0} \tag{22}$$

Therefore, the input acceleration vector for the linear shaker $\underline{\ddot{x}}_{sa}$ is derived by solving the following linear matrix equation:

$$(\mathbf{G}^T\mathbf{G})\,\underline{\ddot{x}}_{sa} = \mathbf{G}^T\underline{z} \tag{23}$$

The LSSS least squares method differs from the transfer function approach in that the least squares approach minimizes the error for the displacement, velocity, and acceleration responses at all DOFs simultaneously. Furthermore, the least squares method can be extended to non-linear response problems provided that a representative, sufficiently accurate and validated non-linear model of the structure is used.

Numerical example

The two motion transformation solutions presented above (the transfer function and least squares methods) are illustrated through a numerical example using the three-story, two-bay planar frame shown in Figure 3. The natural periods and mass ortho-normalized vibration mode shapes are shown in Table I. A damping ratio of 5% was assumed for all the modes, and the linear shaker system is assumed to be attached to the roof as shown in Figure 3. The 1940 El Centro N–S acceleration time history, with acceleration values multiplied by 0.15, was used as the control motion. Amplitude scaling was performed to match the performance specifications of the NEES@UCLA linear shaker, which has the following nominal capacities:

Table I. Modal properties of the example building.

		1st Mode	2nd Mode	3rd Mode
Natural frequency		2.85 Hz	9.26 Hz	16.4 Hz
Mode shapes	Roof floor	2.016	−1.466	−0.673
	2nd floor	1.479	1.251	1.707
	1st floor	0.643	1.719	−1.816

66.75 kN (15 kips) maximum force, ±38.1 cm (±15 inch) stroke and 340.7 lpm (90 gpm) peak flow capacity. The moving mass of this shaker is $m_s = 22.25$ kN (5 kips), and the weight of the fixed parts of the shaker system such as reaction block, hydraulic pump, and plumbing were ignored. Lastly, the linear shaker was assumed to be anchored to the roof and to have perfect tracking of the filtered control motion.

The equation of motion for the structure, given in Equation (2), and the effective lateral force vectors $\underline{f}(t)$ and $\underline{f}'(t)$ from Figure 1 with $n = 3$, were used in this example. Using the transfer function method, four different motion transformations were performed to match the displacement responses of the first, second and third stories, as well as the inter-story drift between the second and third floors. From Equation (12), filters for each response quantity match were derived. For example, filter $T_3(s)$, which equates the roof displacement response for base and top excitation cases can be expressed as:

$$T_3(s) = \frac{H_{31}(s)m_1 + H_{32}(s)m_2 + H_{33}(s)m_3}{m_s H_{33}(s)} \tag{24}$$

The filters $T_1(s)$ and $T_2(s)$ to match the 1st and 2nd floor displacements, respectively, can be derived similarly. To match inter-story drift between floors i and $k = i + 1$, Equation (12) was modified to

$$T(s) = \frac{\sum_{j=1}^{n}(H_{ij}(s) - H_{kj}(s))m_j}{(H_{in}(s) - H_{kn}(s))m_s} \tag{25}$$

For example, filter $T_{32}(s)$, which replicates the relative horizontal displacement between the roof and the 2nd floor (i.e. $\Delta_{32} = x_3 - x_2$), is given by

$$T_{32}(s) = \frac{m_1(H_{31}(s) - H_{21}(s)) + m_2(H_{32}(s) - H_{22}(s)) + m_3(H_{33}(s) - H_{23}(s))}{m_s(H_{33}(s) - H_{23}(s))} \tag{26}$$

The amplitude and phase spectra of filters $T_1(s)$, $T_3(s)$, and $T_{32}(s)$ are shown in Figure 4. Figures 5 to 7 show comparisons between the top excitation displacement response (x_i', solid lines) and the base excitation displacement response (x_i, dashed lines). The three figures show results enforcing a match at the roof level (Figure 5, using $T_3(s)$), the first floor level (Figure 6, using $T_1(s)$) and Δ_{32} (Figure 7, using $T_{32}(s)$).

As shown in Figures 5 to 7, the transfer function method yields excellent agreement (as expected) between the top and base excitation cases for the target response quantity and minor discrepancies for non-target response quantities. For example, in the case where roof displacement is the target response quantity (Figure 5), the roof displacement is a nearly perfect match, whereas the 1st and 2nd story x_i' responses deviate slightly from x_i. Also in

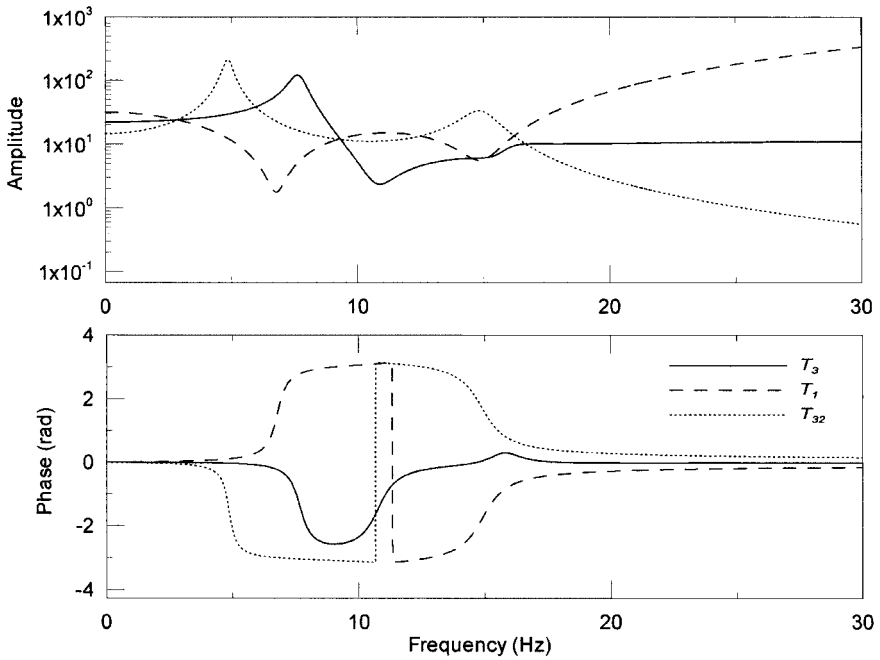

Figure 4. Amplitude and phase spectra of filters ($T_1(s)$, $T_3(s)$, and $T_{32}(s)$).

Figure 6, the 1st floor displacement responses for base and top excitation show a close match. The discrepancy between the top and base excitation responses, herein termed the motion transformation error, can be quantified using a root mean square (RMS) tracking error term defined as

$$\text{RMS tracking error} = \sum_{i=1}^{N} \sqrt{(y_i - y_i')^2} \tag{27}$$

where the summation occurs over time, and y and y' denote generic response quantities for base and top excitations, respectively (e.g. $y, y' = x_n, x_n'$ for roof displacement response). The dimensionless normalized RMS tracking error is defined as the RMS error divided by the RMS value of the base excitation response, which can be expressed as:

$$\text{Normalized RMS tracking error} = \frac{\sum_{i=1}^{N} \sqrt{(y_i - y_i')^2}}{\sum_{i=1}^{N} \sqrt{y_i^2}} \tag{28}$$

Table II presents a summary of normalized RMS tracking errors for the transfer function method examples for each floor level and Δ_{32}. For the transfer function method, the target floor response quantities should theoretically be a perfect match with the base excitation response (RMS error = 0); however, non-zero RMS errors were computed due to numerical errors associated with the discrete Fourier/Laplace transformations. When a local response quantity such as inter-story drift is matched, relatively large discrepancies are observed on global response quantities (floor responses). For buildings with non-uniform mass or stiffness distributions, or with more degrees-of-freedom (i.e. taller structures), the non-target response

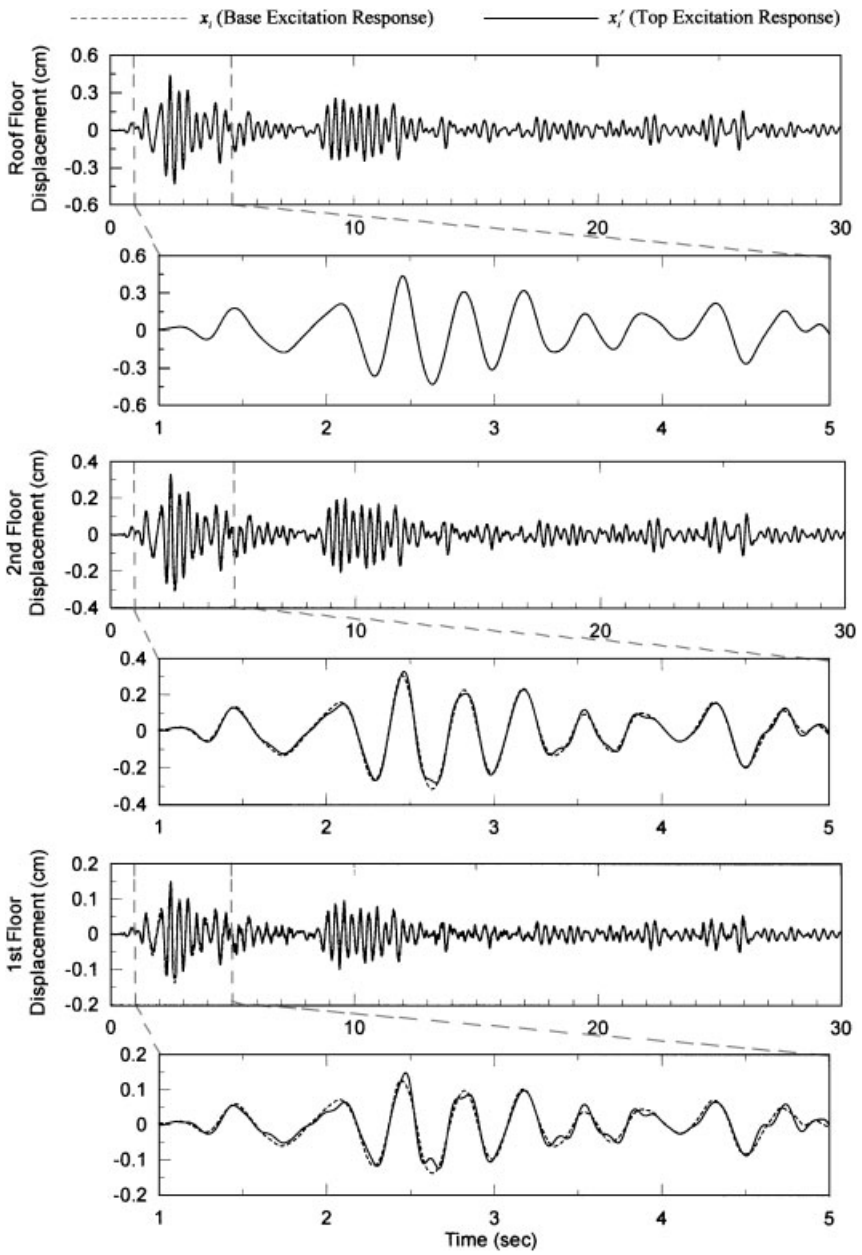

Figure 5. Comparison of base and top excitation responses calculated with the transfer function method (match enforced at Floor 3 using $T_3(s)$).

quantity errors would likely be greater than what is shown in Table II. However, the target response quantity could still be replicated with a high degree of accuracy using the transfer function method.

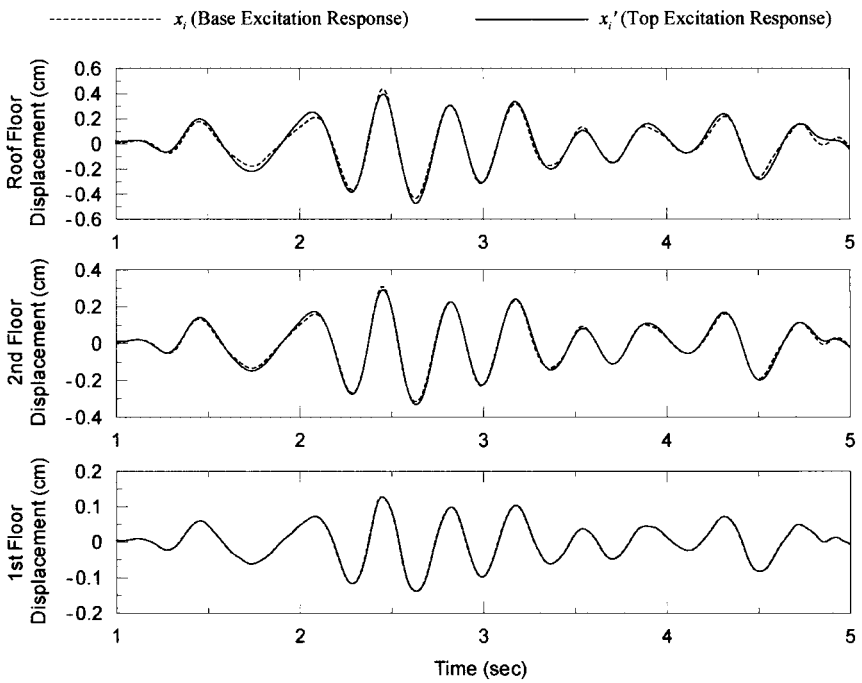

Figure 6. Comparison of base and top excitation responses calculated with the transfer function method (match enforced at Floor 1 using $T_1(s)$).

The motion transformation problem for the example structure in Figure 3 was also solved using the least squares method. The least squares procedure modifies the control motion such that the top-down and bottom-up responses are matched in an average sense in terms of displacement, velocity and acceleration at all degrees-of-freedom. Using Equation (23), a single transformation was performed for the example structure to modify the control motion to simultaneously match as closely as possible all three story displacement, velocity and acceleration responses. Figure 8 shows the displacement responses obtained using the least squares method. As shown in Table II, the least squares method generally minimizes the RMS errors for any particular degree-of-freedom as effectively as the transfer function method. However, the least squares method has the advantage of having consistently small tracking errors for displacement, velocity and acceleration for all three degrees-of-freedom.

THE CONTROL–STRUCTURE INTERACTION PROBLEM

Dyke *et al.* [4] found that the natural velocity feedback loop that exists in hydraulic actuators can cause dynamic coupling between the test structure and actuator. This feedback loop limits the ability of the control system (e.g. controller, servo-valve, and actuator) to provide the flow of hydraulic fluid to the actuator chamber that is required to generate the commanded piston displacement. This effect is accentuated when the response of the test structure is large,

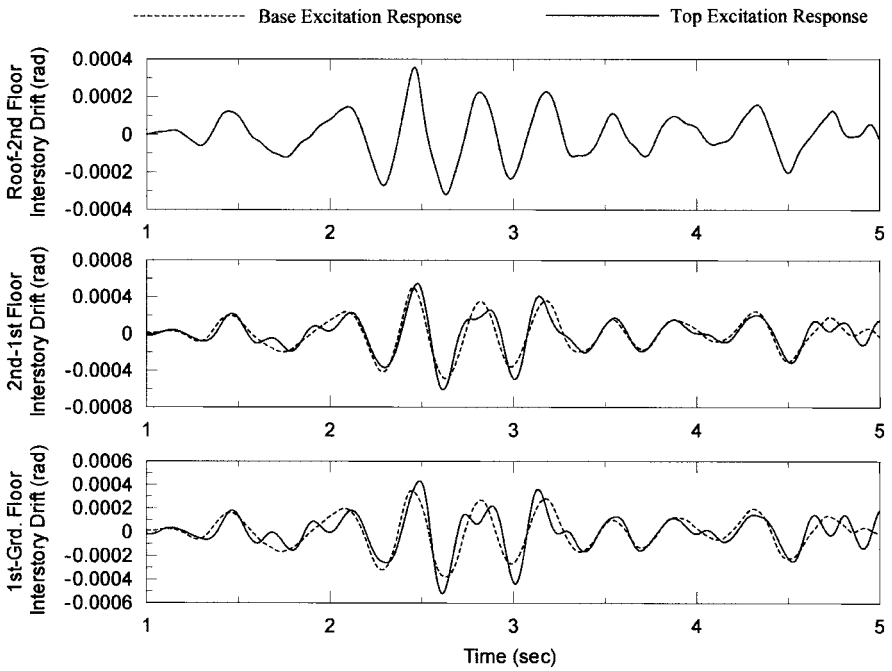

Figure 7. Comparison of base and top excitation interstory drift responses calculated with the transfer function method (enforced match of Δ_{32} using $T_{32}(s)$).

Table II. Normalized RMS tracking errors for each motion transformation.

	TFM (x_1 match)	TFM (x_2 match)	TFM (x_3 match)	TFM[a] (Δ_{32} match)	Least squares method
Roof displacement	0.143	0.082	0.001	0.389 (0.001)	0.043
2nd floor displacement	0.077	0.042	0.126	0.528 (0.442)	0.040
1st floor displacement	0.042	0.108	0.246	0.636 (0.636)	0.116
Roof acceleration	0.913	0.510	0.002	1.094 (0.009)	0.232
2nd floor acceleration	0.165	0.056	0.698	1.499 (1.267)	0.138
1st floor acceleration	0.074	0.801	1.292	1.700 (1.700)	0.292

[a]Values in the parenthesis represent relative displacement or relative acceleration to its lower floor, i.e. Roof–2nd floor relative displacement, 2nd–1st floor relative displacement, etc. from the top.

which occurs near the natural frequencies of the test structure. Accordingly, this dynamic coupling effect, termed control–structure interaction (CSI), can restrict the ability of hydraulic actuators to apply forces near the natural frequencies of the structure. When CSI effects are not accounted for, they can cause significant discrepancies between the desired and achieved system response [2, 4]. Consequently, the LSSS test method consists of two steps: (a) deriving the desired shaker input motion assuming perfect control as previously described, and

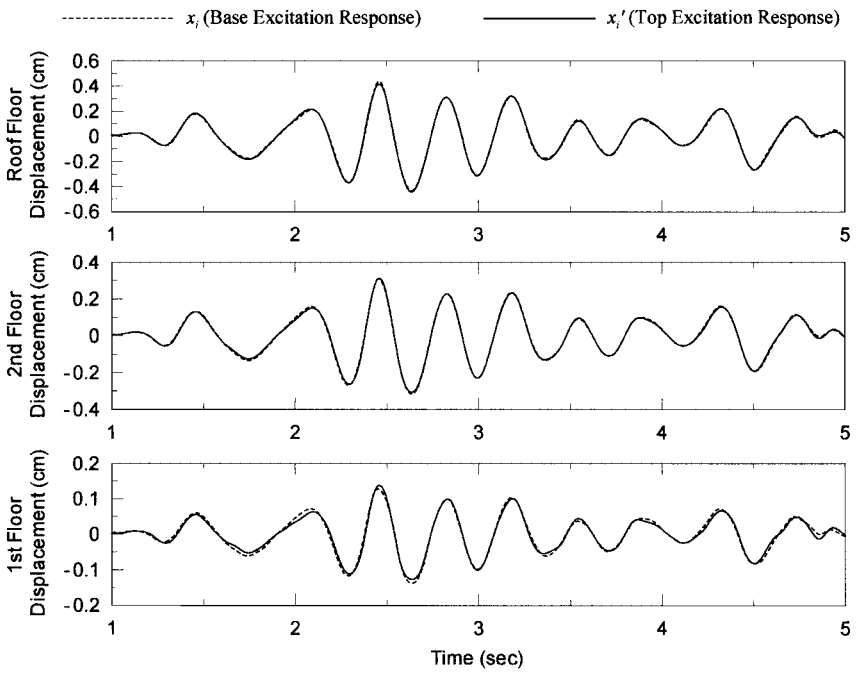

Figure 8. Comparison of base and top excitation displacement responses using the least squares method.

(b) pre-correcting the desired input to compensate for CSI effects. In the following subsections, the analytical methods used to mathematically characterize CSI effects are described and then illustrated with a numerical example.

Linearized model of servo-hydraulic actuator and test structure

A linearized model of both the servo-hydraulic actuator system and the structure to which it is attached is shown in Figure 9. The generic model in Figure 9 is applied here to simulate the performance of the NEES@UCLA servo-hydraulic linear shaker attached to a test structure. Although servo-hydraulic actuation is an inherently non-linear process, a linearized model was used since it has been shown to capture the salient features of the dynamic interactions of the overall system [8, 9]. The block diagram in Figure 9 includes an idealized uni-axial, displacement controlled linear shaker system along with a test structure. System parameters for the NEES@UCLA linear shaker system are summarized in Table III. The oil column frequency of a linear shaker system is given by [8, 10]:

$$f_{\text{oil}} = \frac{A}{\pi}\sqrt{\frac{\beta}{Vm_{\text{s}}}} \tag{29}$$

where $A =$ effective area of actuator piston, $\beta =$ bulk modulus of hydraulic fluid, $V =$ effective volume of actuator cylinder, and $m_{\text{s}} =$ moving shaker mass. Physically, the oil column frequency represents the natural frequency of the hydraulic actuator system, whose stiffness is defined by the oil columns in both actuator chambers (i.e. on both sides of the piston) and

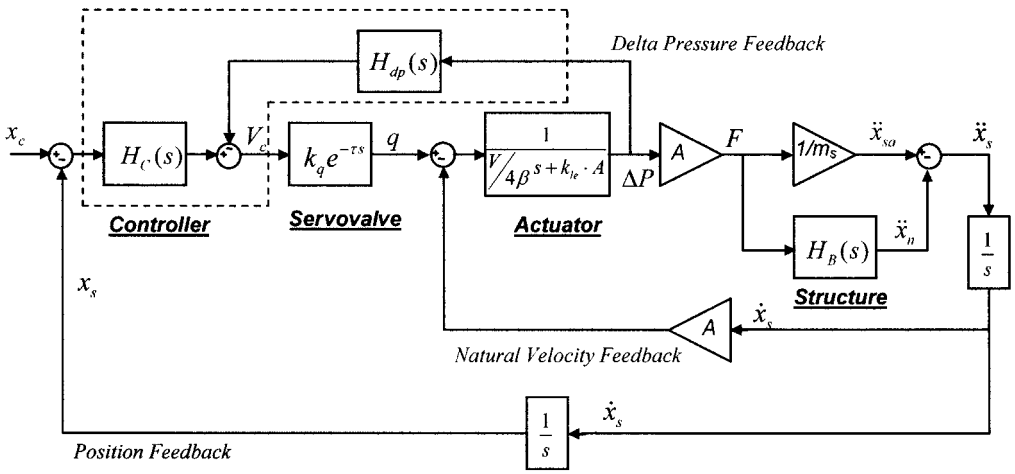

Figure 9. Block diagram model of shaker–structure system.

Table III. Actuator, hydraulic and controller specifications.

Effective volume of both sides of actuator chamber, V	Effective piston area, A	Bulk modulus of hydraulic fluid, β	Flow gain coefficient, k_q
2965.24 cm^3 (180.95 in^3)	33.35 cm^2 (5.17 in^2)	1.585×10^6 kPa (2.3×10^5 psi)	9832.2 $cm^3/s/V$ (600 $in^3/s/V$)

whose mass is given by the moving rigid mass of the shaker (including piston, actuator arm, and swivel). The oil column frequency of the NEES@UCLA shaker is approximately 16 Hz.

The overall system described in Figure 9 consists of several subsystems that are subject to various types of feedback loops as follows:

- **Natural velocity feedback**. The structure displaces when a force is applied by the actuator. Since the actuator cylinder is fixed to the floor of the test building, the movement of the structure/floor results in additional relative displacement between the actuator cylinder and the actuator piston (see Figure 2). This additional movement induces a volume change in both actuator chambers, thereby resulting in a change in the differential oil pressure across the piston, which in turn produces a deviation from the commanded shaker motion. This change in oil pressure, which causes a deviation of the achieved force and displacement from the target values, is referred to as natural velocity feedback. The natural velocity feedback phenomenon exists whether position, force, and/or velocity feedback loops are used to control the shaker (see following button), and causes control–structure interaction to be intrinsic to the device [4].
- **Position feedback**. The actuator piston movement caused by the action of the combined controller-servovalve-actuator-structure system is monitored (as either a displacement, velocity, or acceleration) and is fed back to the controller so that adjustments can be made if the measured response x_s does not match the commanded shaker input

motion x_c. The natural velocity feedback is an important contributor to the difference between x_s and x_c. The NEES@UCLA linear shaker controller uses the displacement of the moving mass as one of the feedback signals to achieve the optimal match between commanded and achieved motion of the moving mass of the linear shaker.

- **Delta pressure feedback**. The displacement of the piston relative to the actuator cylinder occurs due to the pressure differential across the piston. The pressure differential (ΔP) is measured and fed back to the controller, which then adjusts the servovalve command signal V_c based on both the delta pressure feedback signal ΔP and the position feedback X_s. The delta pressure feedback is used to reduce the magnitude of the oil column resonance peak, thus explaining the common reference to delta pressure feedback gain as 'numerical damping'.

We next turn to the modeling of the complete system response. Each of the subsystems with its governing equation is described below.

1. Controller.

$$V_c(s) = H_c(s)[X_c(s) - X_s(s)] - H_{dp}(s)\Delta P(s) \tag{30}$$

As indicated in Equation (30) and Figure 9, the error signal between the commanded shaker input motion $X_c(s)$, and the position feedback (the actual relative position of the moving mass $X_s(s)$), as well as the delta pressure signal (pressure differential), are used by the controller to adjust the servovalve command signal $V_c(s)$. $H_c(s)$ and $H_{dp}(s)$ denote the transfer functions of the controller and delta feedback loop, respectively.

$$H_c(s) = K_p + K_d \frac{s}{s + p_1} \tag{31a}$$

$$H_{dp}(s) = K_{dp} \frac{s}{s + p_2} \tag{31b}$$

Equation (31a) represents a controller model that is referred to as the lead compensator approximation of a proportional-derivative (PD) conditioned control scheme. The PD control is usually adopted to reduce the rise-time and the overshoot of the system response, but pure derivative control is not practical because of the amplification of sensor noise by differentiation and should be approximated by lead compensator form to avoid this problem [11]. In Equation (31b), the transfer function for the delta pressure loop is expressed as another lead compensator approximation for the same reason as in the PD control. In Equations (31), K_p, K_d, K_{dp} denote the proportional, derivative, and delta-pressure control gains, respectively.[‡] These control gains are user-specified, and are adjusted to minimize the tracking error [i.e. the difference between the commanded input position $X_c(s)$ and the actual relative position of the shaker moving mass $X_s(s)$]. Constants p_1 and p_2 designate the pole location of each transfer function. These control gains and constants affect the closed loop response of the system, and are generally determined by trial and error until the target performance criteria are achieved.

[‡] K_d and K_{dp} in Equations (31a) and (31b) are not exactly identical to the conventional derivative gain and delta pressure gain, respectively. The lead compensation approaches pure PD control when a large value is used for the constant p_1 or p_2 [11].

2. Servovalve.

$$Q(s) = k_q e^{-\tau s} V_c(s) \tag{32}$$

Equation (32) describes the oil flow rate into the actuator pressure chamber $Q(s)$ that is generated by the servovalve in response to the servovalve command signal $V_c(s)$ [8]. A linear relationship between $Q(s)$ and $V_c(s)$ is assumed, with the constant of proportionality being the flow gain coefficient k_q, which is a characteristic of the three-stage servovalve used. While a three-stage servovalve has its own feedback loop, this inner control loop was neglected, thus leading the constant flow gain k_q, since servovalve control is significantly more accurate than that of the other subsystems [8, 12, 13]. The time delay τ in Equation (32) is included to model the time necessary to overcome the mechanical and hydraulic inertia of the servovalve.

3. Actuator.

$$Q(s) - sAX_s(s) = k_{le}F(s) + s\frac{V}{4\beta A}F(s) \tag{33}$$

Equation (33) is the flow continuity equation that converts the oil flow rate $Q(s)$ into piston motion $X_s(s)$ and actuator force $F(s)$ [4, 8]. The oil flow rate $Q(s)$ delivered through the servovalve produces a volume change in the actuator pressure chamber, thereby inducing piston movement. However, oil leakage through piston seals (quantified by leakage coefficient k_{le}) and oil compressibility result in additional oil volume changes that must be compensated for by the oil flow rate, thereby reducing the net flow rate as expressed by Equation (33).

4. Structure. The equation of motion in Equation (2) with external force vector taken as $\underline{f}'(t)$ in Figure 1(b).

From the above equations, the transfer function $H_{CSI}(s)$ describing the overall system relationship between the commanded (input) position $X_c(s)$, and the absolute actuator position achieved by the linear shaker $X_{sa}(s)$, can be derived using the transfer function of the servovalve-actuator subsystem $H_s(s)$, and the transfer function of the MDOF test structure $H_B(s)$. This transfer function is referred to herein as the total transfer function of the linear shaker–test structure system, and is given as

$$H_{CSI}(s) = \frac{X_{sa}(s)}{X_c(s)} = \frac{H_s(s)H_c(s)k_q e^{-\tau s}}{1 - H_B(s) + H_s(s)k_q e^{-\tau s}\left[H_c(s)(1 - H_B(s)) + s^2\left(\frac{m_s}{A}H_{dp}(s)\right)\right]} \tag{34}$$

The transfer function $H_s(s)$ describes the relationship between the servovalve output (flow rate $Q(s)$) and the actuator relative displacement $X_s(s)$; therefore, it depends on actuator and structural parameters as

$$H_s(s) = \frac{X_s(s)}{Q(s)} = \frac{1 - H_B(s)}{s^3(Vm_s/4\beta A) + s^2 m_s k_{le} + sA(1 - H_B(s))} \tag{35}$$

The transfer function $H_B(s)$ is derived from the building's equations of motion, Equation (2), taking the absolute acceleration of the moving mass $\ddot{x}_{sa}$ as input and the relative roof acceleration $\ddot{x}_n$ as output, while assuming that the linear shaker is installed at the

roof level. Thus,

$$H_{\mathrm{B}}(s) = \frac{\ddot{X}_n(s)}{\ddot{X}_{\mathrm{sa}}(s)} = -\sum_{i=1}^{n} \frac{m_{\mathrm{s}} \cdot \phi_{ni}^2 \cdot s^2}{M_i (s^2 + 2\zeta_i \omega_i s + \omega_i^2)} \tag{36}$$

where

$\phi_{ni} = n$-th (or roof) component of i-th vibration mode shape
M_i, ζ_i, ω_i = Modal mass, modal damping, and natural circular frequency of the i-th mode.

Numerical example

At this point, it is important to distinguish the different types of errors associated with applying the LSSS test method. Using the previous numerical example (i.e. the structure in Figure 3), we illustrated how a control earthquake ground motion can be modified such that shaker excitation at the roof level replicates the base excitation response with reasonable accuracy assuming perfect actuation. The difference between the base and top excitation responses was termed the motion transformation error, and was attributed to the different inertial force distributions between the base and top excitation cases. The same three-story building is re-analyzed here using the above linearized servo-hydraulic actuator model to characterize the CSI effects. The difference between the achieved and expected (commanded) force outputs in the piston is herein termed the actuation error.[§] Unlike the motion transformation error, the actuation error can be pre-compensated for in the shaker command signal.

For realistic structures, epistemic (or modeling) uncertainties associated with imperfect modeling and characterization of the structure and the servo-hydraulic system may cause further discrepancies in the responses to base and top excitations. Those epistemic uncertainties are not addressed here.

Figure 10 shows the amplitude and phase spectra of the transfer function between input (x_{c}) and output (x_{sa}) of the linear shaker system including the CSI effect, $H_{\mathrm{CSI}}(s)$. These graphs show the transfer function $H_{\mathrm{CSI}}(s)$ in terms of frequency f, which was obtained by substituting $s = i(2\pi f)$ in Equation (34). Notches are observed in the amplitude and phase spectra at the frequencies corresponding to the 1st and 2nd modes of the example building. No permutation is seen near the oil column frequency of 16 Hz (per Equation (29)), which is a result of the derivative and delta pressure gains used in the control algorithm. The main effect of the derivative gain on the hydraulic system is to decrease the oil column frequency, and the effect of the delta pressure gain is to reduce the magnitude of the oil column peak [8]. Because the total transfer function of the linear shaker–structure system [$H_{\mathrm{CSI}}(s)$] is dependent on the hydraulic system parameters as well as the structural parameters of the test structure, optimal control gains are application-dependent. Figure 10 was plotted using control gains determined for the NEES@UCLA linear shaker system under a fixed/stationary base condition.[¶] The control gains were determined by trial and error such that the actual response

[§]In the present paper, we assume displacement control ($x_{\mathrm{s}} = x_{\mathrm{c}}$) of the linear shaker. Thus, the expected (commanded) actuator force implied is $F(t) = m_{\mathrm{s}}\ddot{x}_{\mathrm{s}}(t) = m_{\mathrm{s}}(\ddot{x}_{\mathrm{sa}}(t) - \ddot{x}_n(t))$.

[¶]Values of the control gains and constants used in this paper are: $K_{\mathrm{p}} = 0.472$ V/cm (1.2 V/in), $K_{\mathrm{d}} = 0.591$ V/cm (1.5 V/in), $K_{\mathrm{dp}} = 3.231 \times 10^{-2}$ V/MPa (2.229×10^{-4} V/psi), $p_1 = 1/0.02$ rad/sec, $p_2 = 1/0.07$ rad/sec, $\tau = 0$ sec, and $k_{\mathrm{le}} = 0$ in^3/sec/1b.

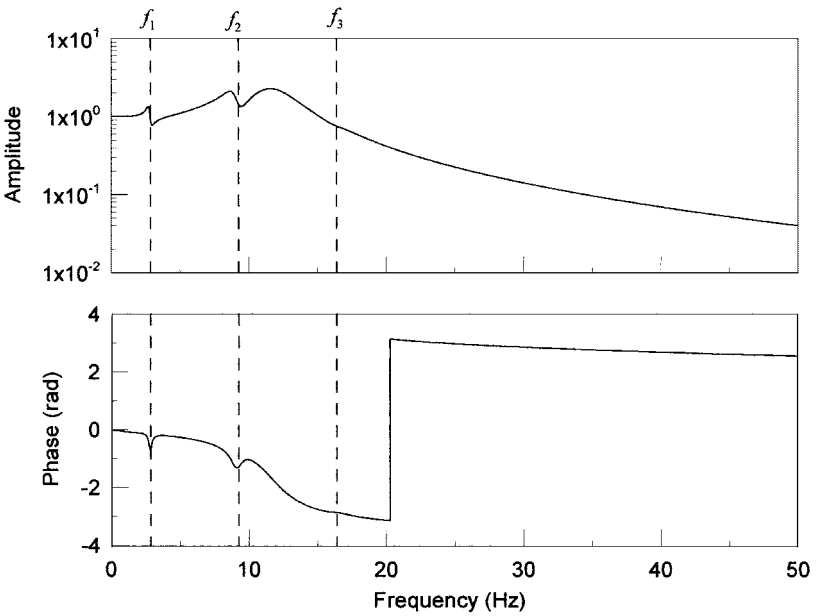

Figure 10. Total transfer function of NEES@UCLA linear shaker in the example building, $H_{CSI}(s)$.

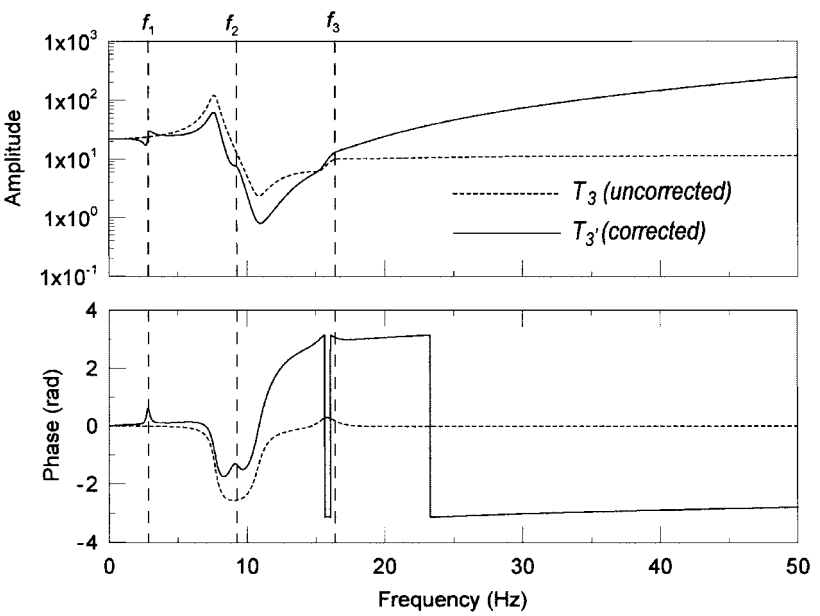

Figure 11. Comparison of amplitude and phase spectra of filter that includes CSI effects (T_3') and that neglects CSI effects (T_3), transfer function method.

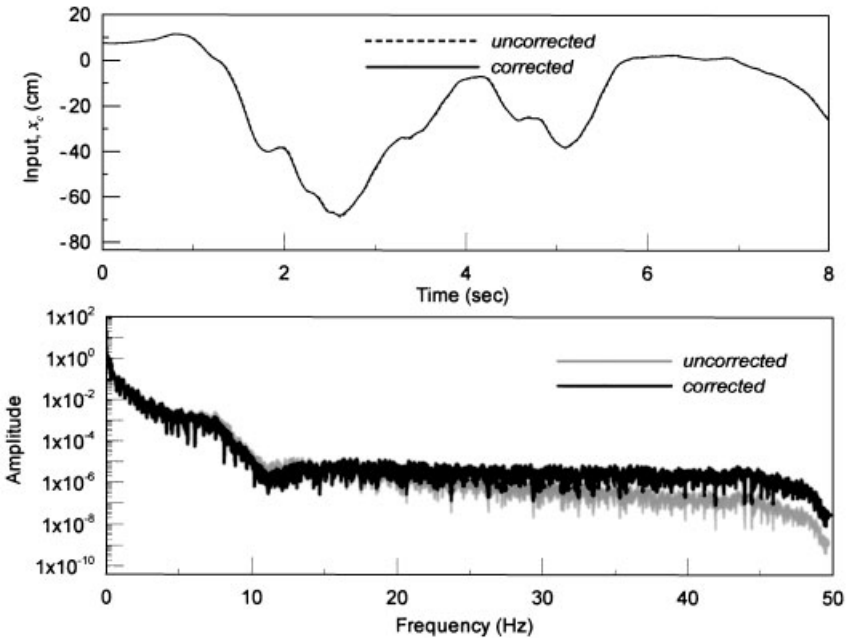

Figure 12. Comparison of shaker input displacement derived using transfer function method with and without correction for CSI effects (T_3 and T_3' for 1940 El Centro control earthquake ground motion).

of the reaction mass $x_{sa}(t)$ closely replicated the command input $x_c(t)$. The optimal gains for a shaker mounted on top of a test structure may be different from those determined while installed on a stationary base. However, the LSSS method has a limited amount of sensitivity to variations of control gains from one application to another, because the CSI effect is pre-corrected in the filtered control motion (using the inverse of $H_{CSI}(s)$) and then is realized as the actuator responds to the command signal (according to $H_{CSI}(s)$). Any differences in the pre-correction CSI transfer function (based on models of the structure and hydraulic system) and the realized CSI effect (by real properties of the structure and hydraulic system) contribute to performance losses of the LSSS method.

Each of the motion transformation filters, which in the previous example were derived using the transfer function method assuming perfect actuation (e.g. T_1, T_3, T_{32}), are now pre-corrected for CSI effects using $H_{CSI}(s)$. For example, $T_3'(s)$ is the CSI-corrected filter that will compensate for the actuation error:

$$T_3'(s) = [H_{CSI}(s)]^{-1} T_3(s) \tag{37}$$

Figure 11 shows the amplitude and phase spectra of the uncorrected filter $T_3(s)$ and CSI-corrected filter $T_3'(s)$. Similarly, the shaker input motion derived using the least squares method, Equation (23), can also be corrected in the frequency domain using $H_{CSI}(s)$. Figure 12 shows a comparison of the shaker input displacement before and after the CSI correction in both the time and frequency domains for the transfer function method when attempting to match the roof displacement response. Figure 13 shows a similar plot for the least squares solution.

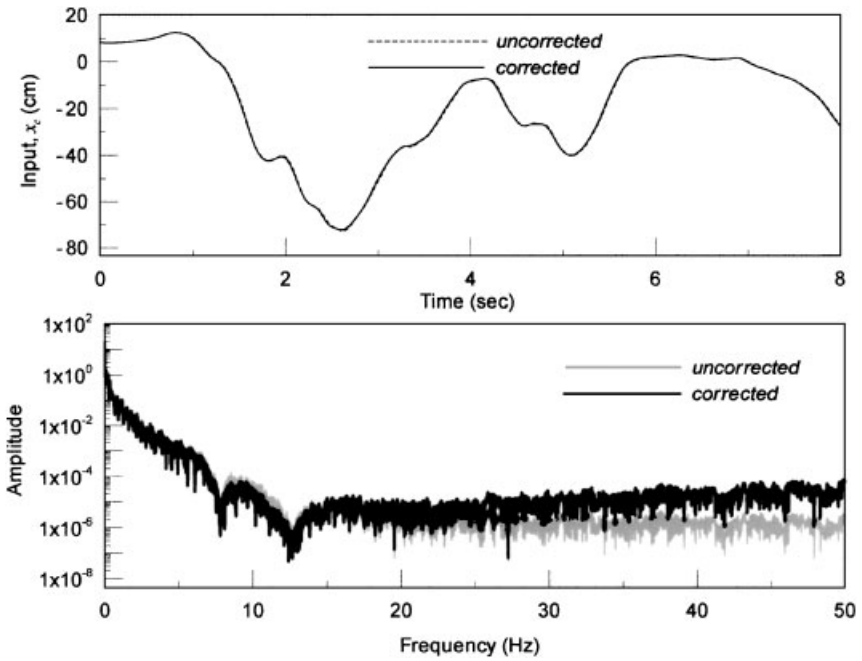

Figure 13. Comparison of shaker input displacement derived using least squares method with and without correction for CSI effects (1940 El Centro control earthquake ground motion).

In Figure 14, we compare the target building response from base excitation (dashed lines) to the response that would be induced by a non-CSI-corrected shaker motion (solid lines). The shaker motion is calculated using the transfer function filter T_3, and the analysis of the resulting building response considers the CSI effect. Figure 15 presents a similar result for the case of a least squares solution of the motion transformation problem. As shown in the figures, the errors associated with neglecting CSI effects in the derivation of shaker motions consist of significant phase differences and small amplitude differences. Those differences result both from imperfect actuation and motion transformation. When the shaker input motion is corrected for CSI effects, the top excitation responses (solid lines) in Figures 14 and 15 are the same as the top excitation responses (solid lines) in Figures 5 and 8, respectively, and the errors in the example are associated only with imperfect motion transformation. As noted previously, for realistic applications, there will be additional discrepancies in building response between the top and base excitation cases due to epistemic uncertainties in the structural and shaker models.

CONCLUSIONS

The linear shaker seismic simulation (LSSS) method is a new method for forced vibration testing of structures to induce dynamic displacement demands that are consistent with earthquake induced shaking at the structure base. This paper addresses two challenges associated

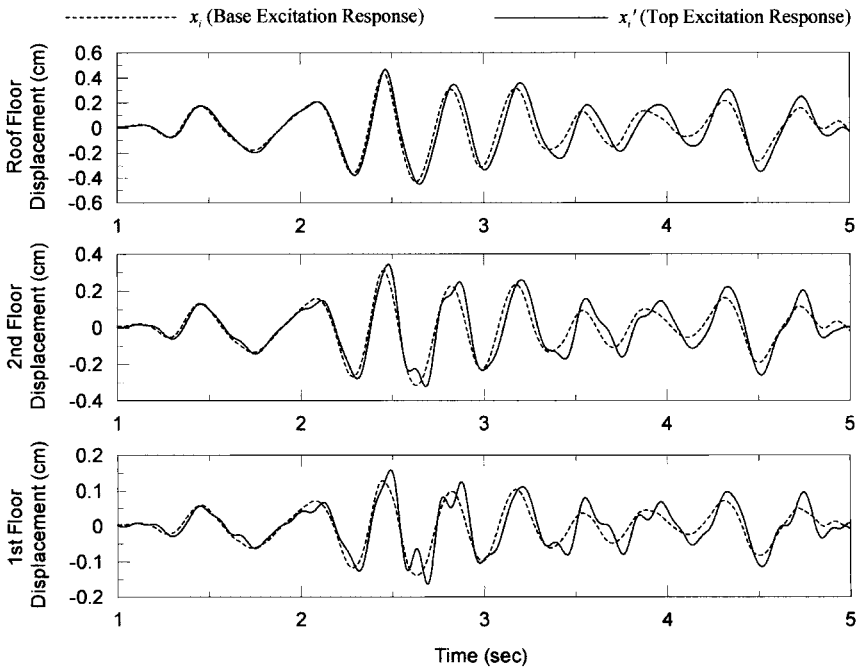

Figure 14. Building displacement response from uncorrected (for CSI effects) input using transfer function method for match of roof floor displacement compared with desired response (for base excitation), El Centro 1940.

with implementation of the LSSS method in the context of linear elastic seismic response for structures. These challenges consist of (a) identifying a linear shaker input motion which produces a structural response similar to that of the building shaken from the base by an earthquake, and (b) pre-correcting the input motion to account for control–structure interaction effects. Procedures for making these corrections have been presented that allow the structural response associated with any particular ground motion time history to be reproduced with top down excitation applied by a linear shaker.

An application of the LSSS method was presented using numerical simulations of the NEES@UCLA linear shaker attached to the roof of a generic three-story test structure. For motion transformation, the 1940 El Centro ground motion was filtered in the frequency domain using the LSSS transfer function approach, as well as in the time domain using the LSSS least squares approach. Analysis results showed that the linear elastic seismic response of low-rise buildings can be replicated with good accuracy once the filtered shaker input motions are pre-compensated for control–structure interaction effects. However, future experimental studies are required to validate this new test method in consideration of unmodeled uncertainties associated with material properties, servo-hydraulic parameters, and modeling of structural and servo-hydraulic shaker systems. In an experimental study involving a real structure, it is crucial that the structural model be as accurate as possible, since this model is used within the motion transformations and CSI correction routines. The model parameters could be most

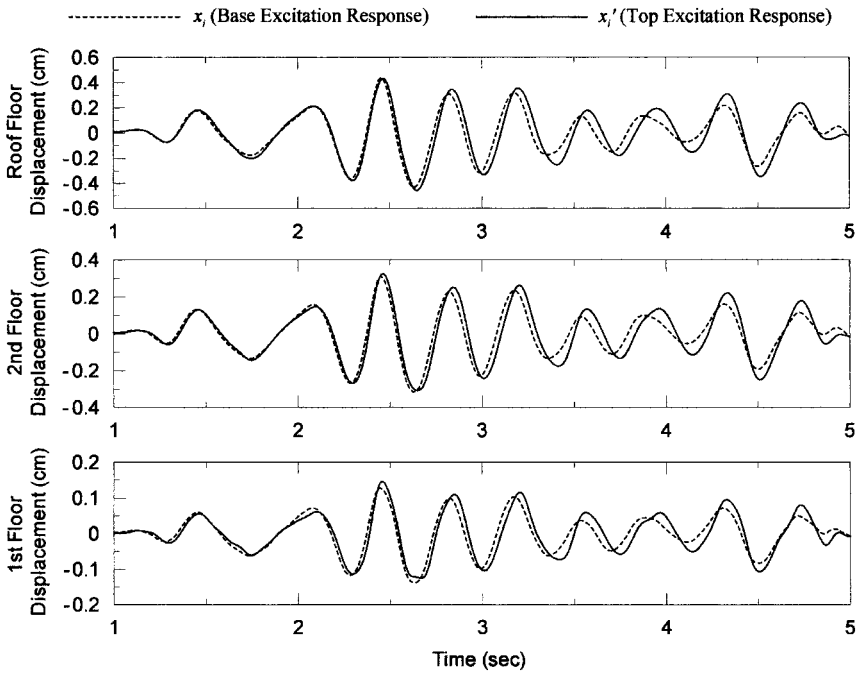

Figure 15. Building displacement response from uncorrected input using least squares method compared with desired response (for base excitation), El Centro 1940.

effectively established through system identification studies making use of pre-test data (such as ambient vibrations).

While such uncertainties may limit the ability of the LSSS method to reproduce the precise response associated with a particular control input ground motion, they should not affect the ability of LSSS testing to provide reliable and repeatable dynamic excitation of test structures across a wide frequency range. It is those issues of reliability and repeatability that are of first-order importance in dynamic structural testing [2]. Lastly, we note that further research is needed to extend the LSSS method for testing of non-linear structures.

NOTATION

The following symbols are used in this paper.

$\mathbf{M}, \mathbf{C}, \mathbf{K}$	mass, damping, stiffness matrix of a structure
m_s	mass of moving part of linear shaker
m_n	story mass of the floor on which linear shaker is installed
$\underline{x}$	displacement response of structure relative to the base
$x_i(t), X_i(s)$	relative displacement response of structure subjected to base excitation
$x_i'(t), X_i'(s)$	relative displacement response of structure subjected to top excitation
$x_s(t), X_s(s)$	displacement of shaker moving mass m_s relative to the floor displacement where shaker is installed

$x_{sa}(t), X_{sa}(s)$	absolute displacement of shaker moving mass m_s
$x_n(t), X_n(s)$	displacement response (relative to building base) of the floor on which linear shaker is installed
$\underline{l}, \underline{l}'$	influence vector in base excitation and top excitation, respectively
$\underline{f}(t), \underline{F}(s)$	effective lateral force vector in base excitation
$\underline{f}'(t), \underline{F}'(s)$	effective lateral force vector in top excitation
$H_{ij}(s)$	transfer function from the j-th floor input to the i-th floor output
$T_i(s)$	motion transformation filter for matching the i-th floor response
$T_i'(s)$	motion transformation filter for matching the i-th floor response (CSI-corrected)
$x_c(t), X_c(s)$	commanded input position of the linear shaker moving mass
K_p, K_d, K_{dp}	proportional, derivative, delta pressure control gains
p_1, p_2	constants designating the pole location of transfer functions of Equations (31a) and (31b)
$x_g(t)$	ground displacement (due to earthquake)
y_i	generic response parameter for base excitation, i.e. displacement, velocity or acceleration responses
y_i'	generic response parameter for top excitation
$\underline{z}$	discrete state vector
$\mathbf{A}, \underline{L}, \underline{L}'$	system matrix and effective load vectors for base and top excitation, respectively
$\mathbf{G}$	$(3nN \times 1)$ matrix used in Equation (19) for calculation of least squares solution
$\underline{\varepsilon}$	error vector containing the difference in responses from base and top excitation
β	bulk modulus of hydraulic fluid
ϕ_{in}	n-th component of the i-th mode shape
ξ_i, ω_i	i-th mode shape, damping ratio, and natural circular frequency of a structure
τ	servovalve time delay
V	effective volume of both actuator chambers (on both sides of the piston)
A	effective area of the actuator piston
k_q	flow gain coefficient of servovalve
$q(t), Q(s)$	flow rate into the actuator pressure chamber
k_{le}	coefficient of leakage across the sealed joints within the actuator
$H_B(s)$	transfer function between the absolute actuator position and the displacement response of the floor on which the shaker is installed
$H_S(s)$	transfer function between flow rate q and actuator displacement x_s
$H_{CSI}(s)$	total transfer function of linear shaker–structure system defined as the transfer function between the commanded input x_c and the achieved absolute actuator position x_{sa}.

ACKNOWLEDGEMENTS

This work was supported primarily by the George E. Brown, Jr. Network for Earthquake Engineering Simulation (NEES) Program of the National Science Foundation under Award Number CMS-0086596. This support is gratefully acknowledged. Any opinions, findings, conclusions or recommendations are those of the authors and do not necessarily reflect the views of the aforementioned organizations.

REFERENCES

1. Joint Technical Committee on Earthquake Protection. *Earthquake Hazard and Earthquake Protection*, Los Angeles, CA, 1993.
2. Dimig J, Shield C, French C, Bailey F, Clark A. Effective force testing: a method of seismic simulation for structural testing. *Journal of Structural Engineering* (ASCE) 1999; **125**(9):1028–1037.
3. Chopra AK. *Dynamics of Structures*: *Theory and Applications to Earthquake Engineering*. Prentice-Hall: Englewood Cliffs, NJ, 1995.
4. Dyke SJ, Spencer BF, Quast P, Sain MK. Role of control–structure interaction in protective system design. *Journal of Engineering Mechanics* (ASCE) 1995; **121**(2):322–338.
5. Stewart JP, Fenves GL. System identification for evaluating soil–structure interaction effects in buildings from strong motion recordings. *Earthquake Engineering and Structural Dynamics* 1998; **27**:869–885.
6. Shing PB, Mahin SA. Pseudodynamic test method for seismic performance evaluation: theory and implementation. *EERC Report UBC/EERC-84/01*, University of California, Berkeley, CA, 1984.
7. Wang YP, Lee CL, Yo TH. Modified state–space procedures for pseudodynamic testing. *Earthquake Engineering and Structural Dynamics* 2001; **30**:59–80.
8. Conte JP, Trombetti TL. Linear dynamic modeling of a uni-axial servo-hydraulic shaking table system. *Earthquake Engineering and Structural Dynamics* 2000; **29**:1375–1404.
9. Trombetti TL, Conte JP. Shaking table dynamics: results from a test-analysis comparison study. *Journal of Earthquake Engineering* 2002; **6**(4):513–551
10. Cundiff JS. *Fluid Power Circuits and Controls*: *Fundamentals and Applications*. CRC Press: Boca Raton, FL, 2002.
11. Franklin GF, Powell JD, Emami-Naeini A. *Feedback Control of Dynamic Systems* (4th edn). Prentice-Hall: Englewood Cliffs, NJ, 2002; 310–315.
12. Rea D, Abedi-Hayati S, Takahashi Y. Dynamic analysis of electro-hydraulic shaking tables. *EERC Report No. 77/29*, Earthquake Engineering Research Center, University of California at Berkeley, CA, 1977.
13. Rinawi AM, Clough RW. Shaking table–structure interaction. *EERC Report No. 91/13*, Earthquake Engineering Research Center, University of California at Berkeley, CA, 1991.

